

Statistical geometry of hard particles on a sphere: analysis of defects at high density

S. Prestipino Giarritta

Dottorato di Ricerca in Fisica, Università degli Studi di Messina, C.P. 50, 98166 S. Agata, Messina, Italy

M. Ferrario and P.V. Giaquinta

Dipartimento di Fisica, Sezione di Fisica Teorica, Università degli Studi di Messina, C.P. 50, 98166 S. Agata, Messina, Italy

Received 27 March 1993

Revised manuscript received 24 June 1993

We analyse the geometry of the solid phase shaped by densely packed hard calottes on a sphere. We show that in this phase topological defects are not distributed at random over the surface but segregate into clusters that give rise to an upper level of organization in the form of a superstructure with icosahedral symmetry.

1. Introduction

In a previous paper [1], henceforth referred to as I, we presented a Monte Carlo study of a two-dimensional system of hard particles embedded on the surface of a sphere. The system consisted of N equal calottes with curved diameter σ . As compared with the phenomenology of hard disks on a plane, the statistical mechanics of this model is largely influenced by the frustration induced on the long-ranged propagation of hexagonal order by the peculiar topology of the host surface.

In paper I we performed a comparative analysis of the translational and orientational correlation functions for different sizes ($N = 400, 1000, 2000$) over a range of densities.

Angular order sets in well before translational order. The initial formation of hexagonal patterns on a local scale is signaled by the appearance in the sixfold orientational correlation function (OCF) $h_6(r)$ of a twin-peak structure corresponding to the second and third coordination shells, respectively, for $\rho\sigma^2 \geq 0.65$. This “fine structure” shows up in the radial distribution function (RDF)

$g(r)$ at much higher densities only, i.e., for $\rho\sigma^2 \geq 0.91$. We note that molecular-dynamics simulations of repulsive *soft* disks did also account for the onset of transient local hexagonal order at about $\frac{7}{10}$ of the freezing density, i.e., for $\rho\sigma^2 \approx 0.62$ [2].

This type of order is reminiscent of a hexatic phase [3]. However, the OCF does not decay at large distances as one would expect for a true hexatic phase. Indeed, in a curved geometry this phase is highly disfavoured, if not totally ruled out, because of the disrupting effect caused by the curvature-induced excess disclinations on long-ranged angular correlations [4]. At high density, such an effect would be even stronger on the hexagonal ordering thus excluding, moreover, the possibility of a discontinuous phase transition. This notwithstanding, the equation of state of the model indicates that calottes undergo a *continuous* transition for $\rho\sigma^2 \approx 0.91$. A tentative characterization of the high-density “solid” phase attained by the system was also given. After noting that hexagonally ordered domains cannot extend along the radial direction further than a critical distance $R_D(N)$, we surmised that the system, in order to achieve maximal efficiency in the packing, promotes an upper level of spatial organization which becomes manifest through the formation of an ordered “superstructure” of domains.

In this paper we plan to extend the analysis carried out in paper I in order to get a deeper insight into the role played by topological defects (such as disclinations and dislocations) in forging the high-density phase of the system. Our theoretical reference will be the KTHNY theory of two-dimensional melting [3]. As a byproduct of this analysis, we shall also clarify the nature of the superstructure attained by the system through a careful scrutiny of the presence of Platonic-tiling modulations in the large-distance behaviour of the distribution functions.

2. Simulation

The details of the numerical experiment were already given in paper I. Here, we just note that one has to be extremely careful on the statistical quality of the Monte Carlo (MC) sampling in the densely packed regime. In particular, in order to achieve reasonable confidence on the reliability of the simulation data in the solid region, we first produced a very long run of about 64000 MC moves per particle at a reduced density $\rho\sigma^2 = 0.925$. We then reshuffled the final configuration through a nonequilibrium “shake” procedure so as to make the system lose any residual “memory” of the initial state. This operation, followed by a standard MC run, was repeated a number of times. Finally, an equilibrium run of 56000 MC moves per particle was performed. Thermo-

dynamic averages were calculated over 1000 configurations, each of them being extracted every $40N$ moves out of the terminal segment of the MC trajectory.

3. Statistics of point defects

In order to describe the local microscopic structure and coordination geometry that characterize the system, it is useful to identify the nearest neighbours of each particle in a given configuration. As discussed in paper I, this task can be accomplished by resorting to the Voronoi tessellation [5]. Fig. 1 shows the distribution of the edge lengths of n -sided Voronoi polygons (with n ranging from 4 to 8) for two values of the reduced density. It clearly emerges that heptagons and octagons are highly distorted as a substantial fraction of these polygons has sides with lengths widely dispersed between zero and the maximum. Furthermore, it is interesting to note that, for increasing densities, the peak of the edge distribution function for heptagons moves from the position of the maximum attained by hexagons towards that of pentagons. This behaviour does indeed suggest the existence of some sort of geometrical

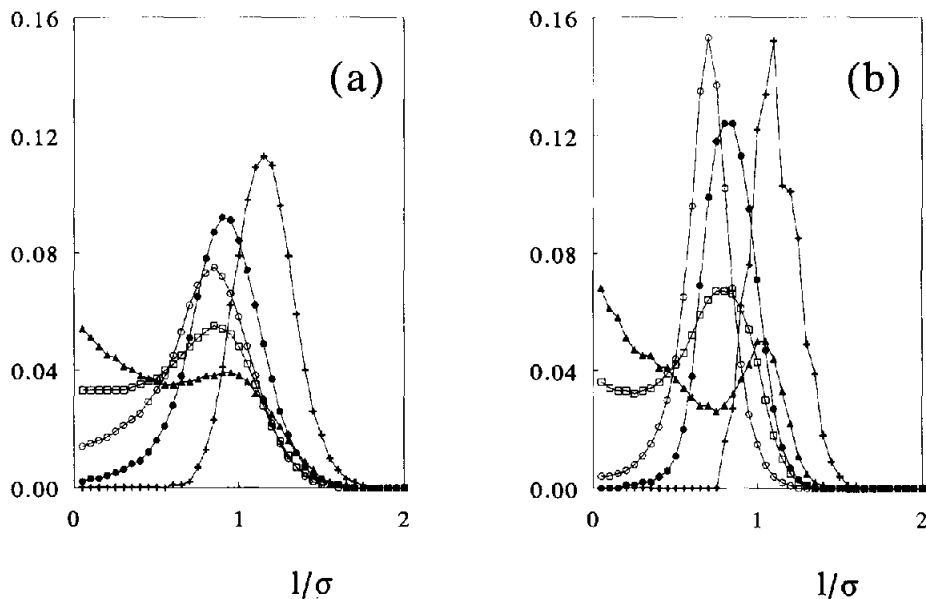


Fig. 1. Statistics of the side lengths of the Voronoi polygons at two densities, (a) $\rho\sigma^2 = 0.75$ and (b) $\rho\sigma^2 = 0.91$, for $N = 2000$. Crosses, solid circles, open circles, squares and triangles refer to 4-, 5-, 6-, 7-, and 8-sided polygons, respectively. The normalization is such that the plotted quantity yields the average frequency of occurrence of a given length (to within $\pm 0.025\sigma$) relative to the total number of instances in a class of polygons.

association between heptagons and pentagons at high density. Correspondingly, the distribution function for hexagons becomes fairly symmetrical.

Once the particles have been classified according to their coordination number, “point defects” can be unambiguously identified: more specifically, we shall refer to a particle surrounded by n nearest-neighbours (with $n \neq 6$) as an n -fold disclination. We recall that the binding of disclinations to form 5–7 “dipoles” (dislocations) is the mechanism that is called for in order to explain the formation of the hexatic phase within the KTHNY theory of melting in 2D [3]. However, more complex defective structures may indeed play a role in the process of ordering such as “rings” (bound pairs of oppositely oriented dislocations) and “grain boundaries”, i.e., chains of alternating 5’s and 7’s.

By joining all the pairs of nearest-neighbour atoms one obtains a network called the “Delaunay net” [5]. In this network, a set of three calottes that are contiguous to one another forms a spherical triangle. Each “edge” (in fact, a geodesic arc) of the triangle will be referred to as a “bond” on merely geometrical grounds. Such close-packed triangles cover the whole surface giving rise to the “Delaunay tessellation”. The Voronoi and Delaunay tessellations are dual to each other.

The numbers of disclinations with different “valency” occurring on the sphere for a given configuration can be related to each other through the Euler formula as applies to any simply-connected surface [6]:

$$V - E + F = 2, \quad (1)$$

where V is the number of vertices in the Delaunay net (equal to the total number of calottes N), E is the number of edges, and F is the number of triangular tiles. Since each edge is shared by two triangles, it follows $2E = 3F$. We can also make use of an extra closure relation after noting that, since n triangles meet at an n -fold coordinated vertex and each triangle belongs to three vertices, the total number of tiles is

$$F = \frac{1}{3} \sum_n nV_n, \quad (2)$$

where V_n is the number of n -fold coordinated vertices. One thus obtains for the average coordination number,

$$\bar{Z} \equiv \frac{1}{N} \sum_n nV_n = 6 - \frac{12}{N}, \quad (3)$$

a result that had been already derived by Nelson using different arguments [4].

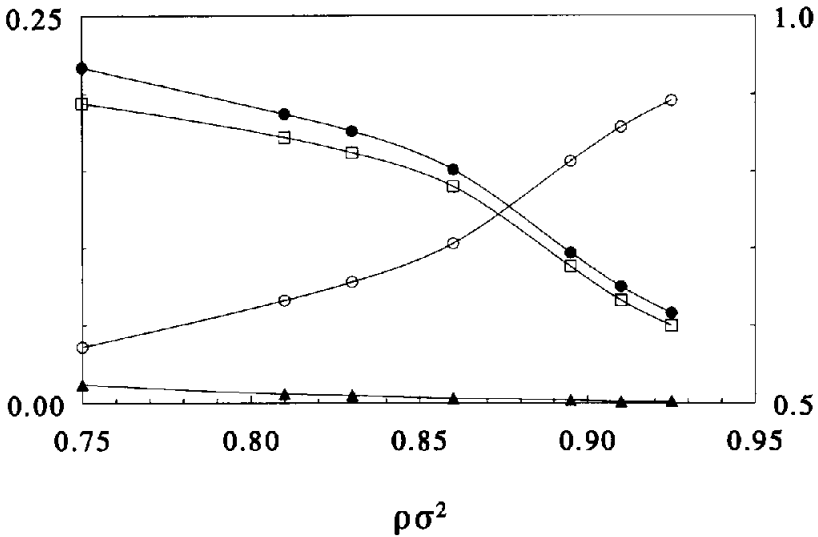


Fig. 2. Average molar fraction of particles with n neighbours as a function of the density, for $N = 2000$; solid circles, $n = 5$; open circles, $n = 6$ (right axis); squares, $n = 7$; triangles, $n = 8$.

If we let the radius of the sphere increase indefinitely (and, correspondingly, $N \rightarrow \infty$), we recover the limit of an infinite plane.

In fig. 2 we show the average molar fractions of n -fold coordinated calottes,

$$x_n = \frac{\langle V_n \rangle}{N}, \tag{4}$$

as a function of the reduced density $\rho\sigma^2$ for $N = 2000$. We first note that the number of particles with six neighbours rises almost linearly up to $\rho\sigma^2 \approx 0.83$: beyond this threshold x_6 starts to increase much more rapidly, thus indicating the outburst of hexagonal order in the system. Correspondingly, beyond $\rho\sigma^2 \approx 0.86$ we observe a drastic drop in the number of fivefold and sevenfold disclinations. On the sphere, at intermediate densities, most of these defects are grouped together, the number of isolated 5's and 7's never exceeding 2% of the total number of point defects. The excess of fivefold over sevenfold disclinations also decreases for increasing densities, eventually tending to the value of 12 as demanded by Euler's formula.

Fourfold and eightfold disclinations are a minor fraction and, at high density, appear only in a few peculiar patterns. In particular, we observe that a fourfold disclination usually links to a sevenfold coordinated particle. The fourfold head of the resulting dipole takes the place of a fivefold disclination inside a chain of alternating 5's and 7's. Instead, eightfold disclinations appear to play the role

of “counter-defects” with respect to the 5’s in that they bind a triplet of 5’s in a sort of starlike arrangement, which, moreover, induces a depression of the local density. On account of the above evidence, the “effective” numbers \tilde{V}_5 and \tilde{V}_7 of fivefold and sevenfold disclinations that are not bound to the 8’s and 4’s, respectively, may be estimated as

$$\tilde{V}_5 = V_5 - 3V_8 + V_4, \quad (5)$$

$$\tilde{V}_7 = V_7 - V_4. \quad (6)$$

Using eq. (3), we find

$$\tilde{V}_5 - \tilde{V}_7 = 12 - V_8. \quad (7)$$

For increasingly dense packings disclinations other than 5’s and 7’s progressively disappear since a greater and greater efficiency is requested in the way particles are distributed over the surface. In this regime, which settles down for $\rho\sigma^2 \geq 0.91$, eq. (7) yields asymptotically $V_5 - V_7 = 12$, in contrast to what would occur in a 2D flat space where eq. (3) leads to equal numbers of fivefold and sevenfold disclinations. The excess of 5’s over 7’s on the sphere is clearly induced by the curvature of the surface and is superimposed over a sea of thermally activated defects. Upon decreasing the density, a larger and larger number of excess fivefold disclinations are “neutralized” by the 8’s whose number gradually increases. At the same time, fourfold and eightfold disclinations give rise to more complex aggregates than those discussed above. Correspondingly, the estimates of \tilde{V}_5 and \tilde{V}_7 given in eqs. (5) and (6) become less and less realistic. We verified that for 2000 particles eq. (7) keeps valid for densities down to $\rho\sigma^2 \approx 0.83$, where the average number of eightfold disclinations becomes equal to 12. As a result, the excess of residual fivefold disclinations vanishes and the statistics of defects becomes largely similar to that on a plane. In fact, it is roughly at such a density that the EOS of calottes merges into that of hard disks [1]. For lower densities, counting how many 5’s and 7’s are effectively bound by eightfold and fourfold disclinations becomes far from trivial. However, we expect that the condition $\tilde{V}_5 \approx \tilde{V}_7$ keeps true on the average.

Aside from isolated disclinations and dislocations, we systematically monitored linear defective structures such as grain boundaries and dislocation pairs with or without an attached tail of alternating 5’s and 7’s. The rest of point defects appear in the form of clusters with a far more complex shape. The fraction of defects belonging to these clusters is bigger than 90% for $\rho\sigma^2 = 0.75$ and drops below 50% for $\rho\sigma^2 = 0.91$. We observe that, within the restricted

ensemble of linear defects only (thereby including also bound dislocation pairs), the percentage of defects forming dipoles and grain boundaries gradually increases with the density up to a value of about 80% for $\rho\sigma^2 \approx 0.83$, hereafter keeping roughly constant. This density marks indeed the beginning of a deeper structural transformation undergone by the system as can be better appreciated by looking at some other indicators that are rather sensitive to the establishment of extended translational order. In particular, we refer to the pairing of dislocations, a process that in the KTHNY theory is invoked as the mechanism leading to the formation of the solid phase.

From a topological point of view, a spatially coherent hexagonal tessellation of the surface is not disrupted by the presence of a bound dislocation pair: in fact, this composite defect does not interfere heavily with the surrounding structure. This should be contrasted with the effect induced by an *isolated* 5-7 dipole (a dislocation) which, in a triangular lattice, is associated with the appearance of two additional half-rows of atoms meeting at the fivefold vertex and forming an angle of 60° . Actually, this lattice deformation may be compensated by an opposite dipole lying farther away. Isolated dislocations lead to a substantial breaking up of the translational order in the system. On the other hand, their effect is less dramatic on the propagation of orientational order. Fig. 3 shows the number of disclinations belonging to rings relative to the population of point defects forming linear defects. We note that the fraction

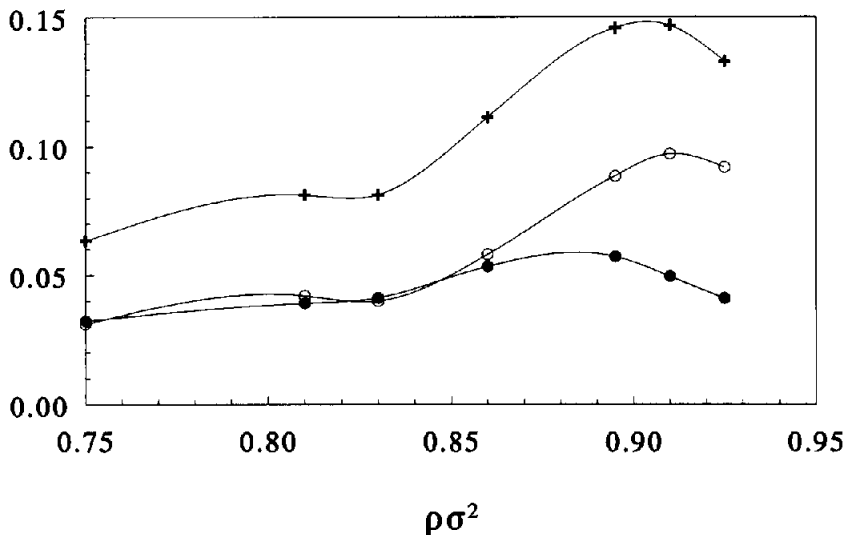


Fig. 3. Average number of disclinations forming "rings" (see text) plotted as a function of the density for $N=2000$. This number is referred to the total number of linear defects at a given density, rings included. The solid and open circles refer to rings with or without a tail of alternating 5's and 7's. The crosses give the sum of the two contributions.

of rings sharply increases for $\rho\sigma^2 \approx 0.83$ at the expense of the residual isolated disclinations. This growth is mainly ascribable to rings without a tail and saturates for $\rho\sigma^2 \approx 0.91$, i.e., in correspondence with the claimed transition of the system to a fully ordered state. Had we also included the fraction of distant oppositely oriented dipoles, this effect would have been even stronger.

It clearly emerges that the overall nature of the topological defects found in this model is considerably more complex than in the KTHNY picture as, moreover, already observed by a number of authors for other 2D systems (see, for example, [7]). Nevertheless, on the basis of the above evidence on the behaviour of paired dislocations, we surmise that the system undergoes a *diffuse* freezing transition over a range of densities ($0.83 \leq \rho\sigma^2 \leq 0.91$), a transition which culminates with the formation of an orientationally and translationally ordered structure.

4. Defect radial distribution functions

As emphasized in the introduction, the spatial organization of point defects is crucial for understanding the geometry of the phase attained by the model at high densities. In order to solve this problem, we resort to the calculation of pair distribution functions between particles with given coordination:

$$\rho_\alpha \rho_\beta g_{\alpha\beta}(r) = (1 + \delta_{\alpha\beta}) \frac{\langle \mathcal{N}_{\alpha\beta}^{\text{pairs}}(r) \rangle}{\mathcal{A} \mathcal{S}(r)}, \tag{8}$$

where $\mathcal{N}_{\alpha\beta}^{\text{pairs}}(r)$ is the number of distinct pairs of particles with coordination numbers α and β lying at a distance between r and $r + \Delta r$ (with $\Delta r \ll \sigma$), $\mathcal{S}(r) = 2\pi R \sin(r/R) \Delta r$ is the area of a spherical ring with curved radius r and thickness Δr , $\mathcal{A} = 4\pi R^2$, $\rho_\alpha = \langle N_\alpha \rangle / \mathcal{A}$ is the average partial density of particles of species α , and $\delta_{\alpha\beta}$ is Kronecker's symbol. The average in eq. (8) is carried out over the configurations sampled for a fixed total number density ρ .

Eq. (8) leads to the "spectral decomposition" of the full pair distribution function $g(r)$ in the form

$$g(r) = \sum_{\alpha,\beta} x_\alpha x_\beta g_{\alpha\beta}(r), \tag{9}$$

where $x_\alpha = \rho_\alpha / \rho$.

Fig. 4 shows the comparison between the RDF of 2000 calottes for $\rho\sigma^2 = 0.925$ and the RDF of sixfold coordinated particles only. As expected, the presence of defects in the hexagonal texture of the surface leads to a systematic softening of the spatial profile of the full $g(r)$ as compared with that of $g_{66}(r)$.

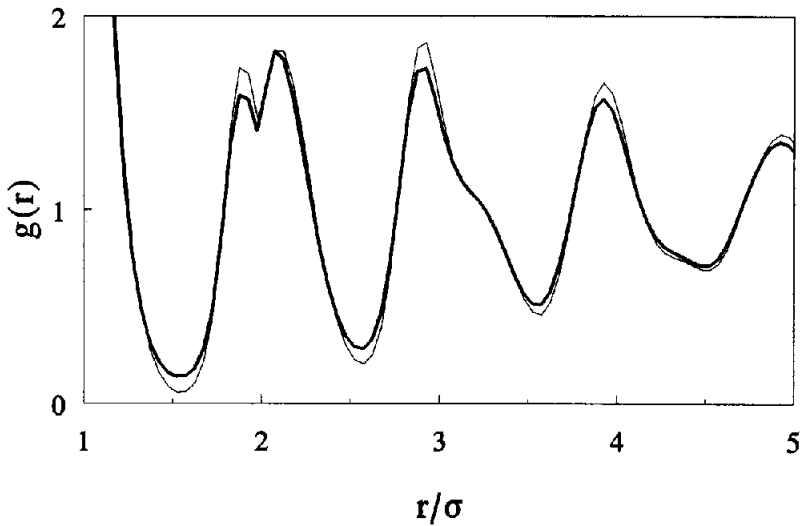


Fig. 4. Radial distribution of 2000 calottes (thicker line) compared with $g_{66}(r)$ for $\rho\sigma^2 = 0.925$.

The distribution functions associated with fivefold and sevenfold disclinations are shown in fig. 5. We start noting the presence of an “interstitial” peak in both $g_{55}(r)$ and $g_{77}(r)$ in a range of distances corresponding to the first dip in $g(r)$. We verified that these structures are associated with interparticle separa-

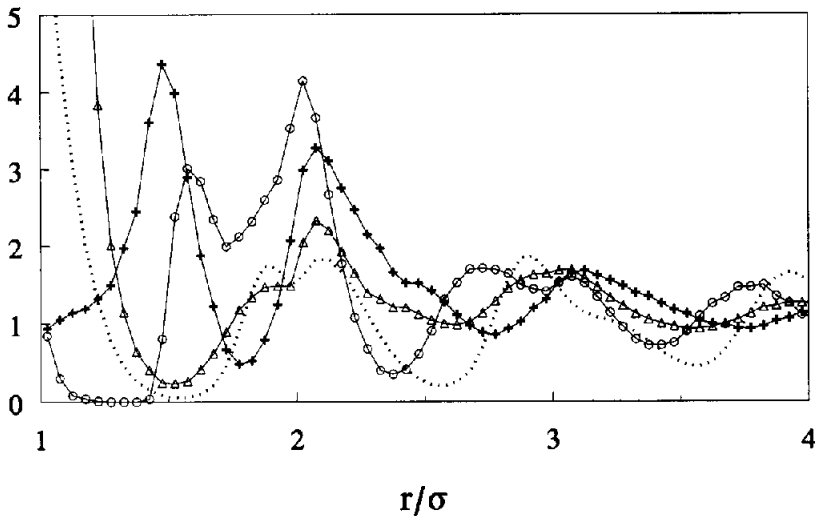


Fig. 5. Radial distribution functions of fivefold and sevenfold disclinations for $\rho\sigma^2 = 0.925$ and $N = 2000$: open circles, $g_{55}(r)$; crosses, $g_{77}(r)$; triangles, $g_{57}(r)$. The function $g_{66}(r)$ is also shown as a dotted line for comparison.

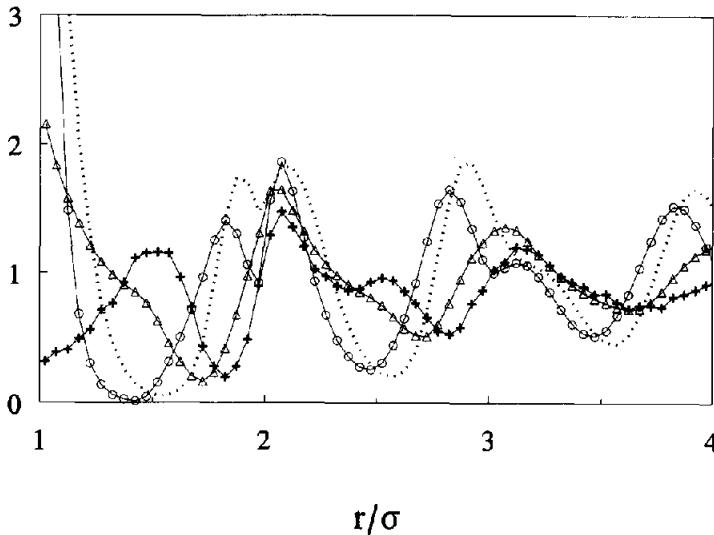


Fig. 6. Cross radial distribution functions $g_{6\alpha}(r)$ for $\rho\sigma^2 = 0.925$ and $N = 2000$: circles, $g_{65}(r)$; dots, $g_{66}(r)$; triangles, $g_{67}(r)$; crosses, $g_{68}(r)$.

tions in a ring. The next maxima at $r/\sigma = 2.1$ arise from next-nearest-neighbour separations within a chain 5–7–5–... and fall on top of the third-neighbour peak in $g(r)$. However, a more impressive match with the prevailing hexagonal distribution is found in $g_{57}(r)$. The rather close correspondence of peaks and dips in this function with those in $g_{66}(r)$ shows that the linear structures formed at high density by alternating 5's and 7's fit rather well the triangular periodicity over the surface. We also note that the contact value of $g_{57}(r)$ rapidly increases with the density and eventually blows up thus indicating the ever increasing stability of the dipolar 5–7 bond on approaching the solid phase. Fig. 6 finally shows the cross correlations between sixfold particles and disclinations. Whereas the 6–5 profile merely anticipates the spatial modulation of $g_{66}(r)$, the appearance of interstitial structures becomes more and more evident in $g_{67}(r)$ and $g_{68}(r)$.

5. The structure of the solid phase

In paper I we had already observed that the long-range decay of the RDF is distinctly modulated at high density by a superimposed periodicity with a wavelength much larger than the hard-core diameter σ . This behaviour was related with the formation of a superstructure with a high degree of symmetry embodying extended hexagonal patches. As a result, we argued that defects

would likely segregate inside the interstices between such ordered domains thus giving rise to a *dual* frame. It is precisely the pinning down of this superstructure that completes the ordering process of the system with a continuous transition at $\rho\sigma^2 \approx 0.91$.

In order to characterize the large-scale geometry of the solid phase we analyse the long-range behavior of the cumulative RDF of point defects $g_{\text{def}}(r)$, which bears the most distinct signature of the hidden frame:

$$g_{\text{def}}(r) \equiv \frac{\sum_{\alpha, \beta \neq 6} x_\alpha x_\beta g_{\alpha\beta}(r)}{\sum_{\alpha, \beta \neq 6} x_\alpha x_\beta} \tag{10}$$

This function, evaluated for $N = 2000$, is presented in fig. 7 for three densities across the transition point. The long-wavelength modulation observed in $g_{\text{def}}(r)$ acquires a definitive shape beyond $\rho\sigma^2 \approx 0.91$. This modulation, which is absent for $\rho\sigma^2 < 0.895$, is a clear imprint of the nonuniform distribution of defects on the sphere. In order to identify the geometry of the frame underpinning clusters of defects at high density, we shall consider some *model* distributions of “continuous matter” over the surface so as to mimic the space partitioning between sixfold coordinated particles and defects. We shall investigate some highly symmetrical arrangements only, corresponding to the

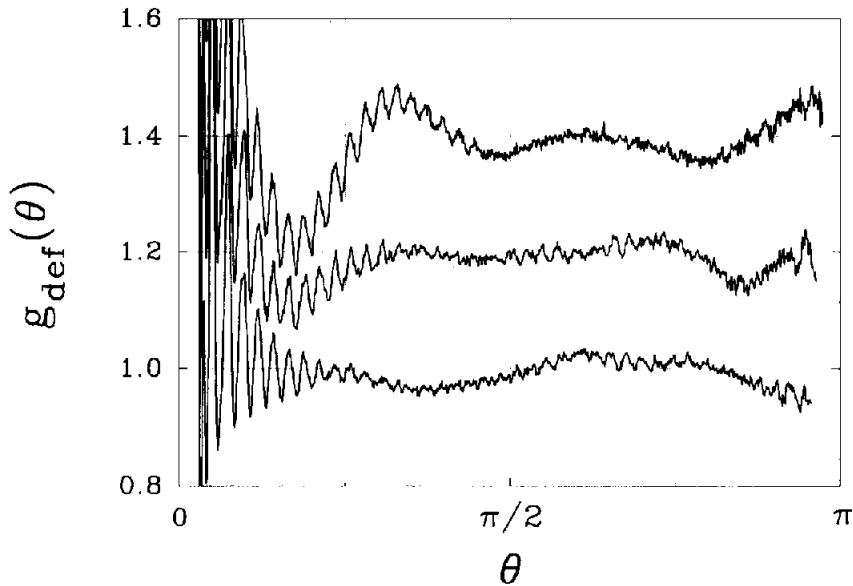


Fig. 7. Cumulative radial distribution function of defects plotted as a function of the angular distance $\theta = r/R$ at three densities ($\rho\sigma^2 = 0.895, 0.91, 0.925$) for $N = 2000$. The density increases from bottom to top, each successive curve being displaced upwards by 0.2 for clarity.

Platonic polyhedra inscribed within the sphere. Hexagonally ordered domains are represented by equal, extended calottes (not to be confused with the “constituent” particles of the system) centred at the vertices of a regular polyhedron \mathcal{P} . The space left over between these circular domains, which may also overlap, is made up by small islands with a curved polygonal shape and has the symmetry of the polyhedron $\hat{\mathcal{P}}$ dual to \mathcal{P}^{*1} . This space is associated with a uniform distribution of defects whose RDF is computed as

$$g_I(r) \equiv \frac{\langle a_1(P; r) \rangle_{P \in I}}{\mathcal{S}(r) \eta_I} \tag{11}$$

In eq. (11) P is a point in the interstitial region I , $\mathcal{S}(r)$ is the area of a spherical ring centred at P with curved radius r and thickness Δr , η_I is the ratio of the total area covered by the interstices to the area of the spherical surface, and the quantity $a_1(P; r)$ is the area of the ring portion that is contained within the interstitial region. The average is carried out by sampling a statistically significant set of points over this region. Within such a simplified scheme, one might also consider the interdomain distribution function $g_D(r)$. Its definition is entirely analogous to that of $g_I(r)$ in eq. (11), the only difference being that the point P lies inside a circular domain. However, it is not difficult to verify that the two functions are trivially related:

$$g_D(r) = \frac{1 - 2\eta_I}{(1 - \eta_I)^2} + \left(\frac{\eta_I}{1 - \eta_I} \right)^2 g_I(r) \tag{12}$$

Therefore, the shape of the two functions is absolutely the same.

Fig. 8 shows the interstice RDF’s computed for defect distributions, each endowed with a symmetry corresponding to one of the five Platonic polyhedra. In this calculation domains were assumed to be tangent to each other. A comparison of these model RDF’s with the defect RDF’s that are reported in fig. 7 does provide a clue for understanding the nature of the superstructure attained by the system at high densities. In fact, we can envisage the initial sprouting of a *tetrahedral* clustering of defects which, across the transition, appears to evolve into an *icosahedral* structure (see footnote 1). The presence, on the average, of twelve clusters of defects is consistent with the asymptotic expectation of twelve unpaired disclinations on the sphere. Furthermore, the segregation at the vertices of an icosahedron ensures the maximum relative distance between neighbouring clusters, a condition that allows an optimal

*1 We recall that the tetrahedron is dual to itself, the cube and the octahedron are dual to each other, while the dodecahedron is dual to the icosahedron (and vice versa).

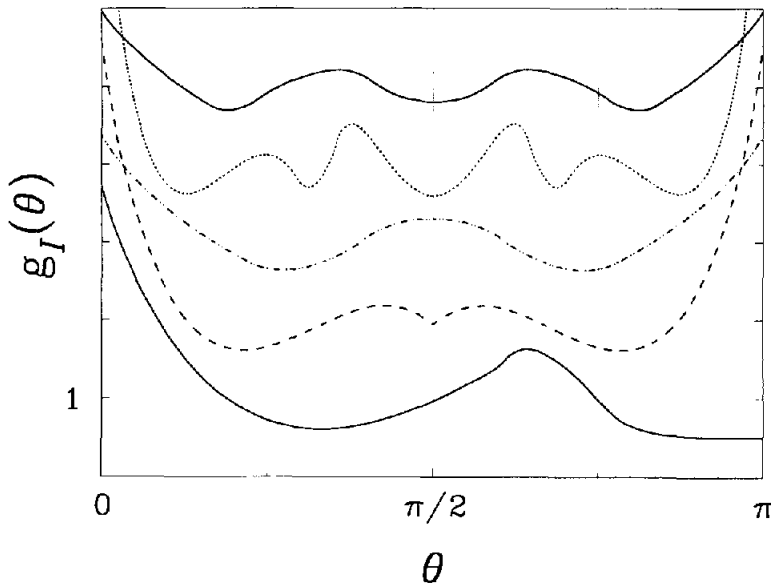


Fig. 8. Interstice radial distribution function $g_I(r)$ plotted as a function of $\theta = r/R$ for Platonic distributions of “matter” on the sphere. Matter is uniformly distributed inside equal circular domains which are centred at the vertices of a regular polyhedron inscribed within the sphere. Domains are tangent to each other. Each successive curve is displaced upwards by 2 for clarity. From bottom to top: tetrahedron, octahedron, cube, icosahedron, and dodecahedron.

spreading of connected hexagonal patches through the surface [8]. We have also verified that the correspondence between the model calculation for an icosahedral frame of defects and the true $g_{\text{def}}(r)$ at high density is independent on the details of the geometrical construction. In fact, if we increase the size of the circular domains (which, in this case, are centred at the vertices of a dodecahedron), the interstitial region breaks into disjoint islands with a decreasing area. Such a geometry is somewhat more representative of the real distribution of defects which appear to be rather confined and immersed into a pervading sea of sixfold coordinated particles (see fig. 10 of paper I). Fig. 9 shows how the profile of $g_I(r)$ changes upon shrinking the spatial extension of the interstices. We note that the amplitude only of the oscillations is affected by the different geometrical setup while the modulation is absolutely preserved.

Obviously, an alternative choice to the model distribution discussed above might as well be that of associating the surface occupied by defects with the circular domains centred at the vertices of the inscribed polyhedron, rather than with the interstices. In this case, one should exploit the potential correspondence of the *domain* RDF, $g_D(r)$, with $g_{\text{def}}(r)$. In fig. 10 we present the result of such a calculation in the case of an icosahedral frame. A comparison with fig. 9 shows that, if the domains are tangent to each other,

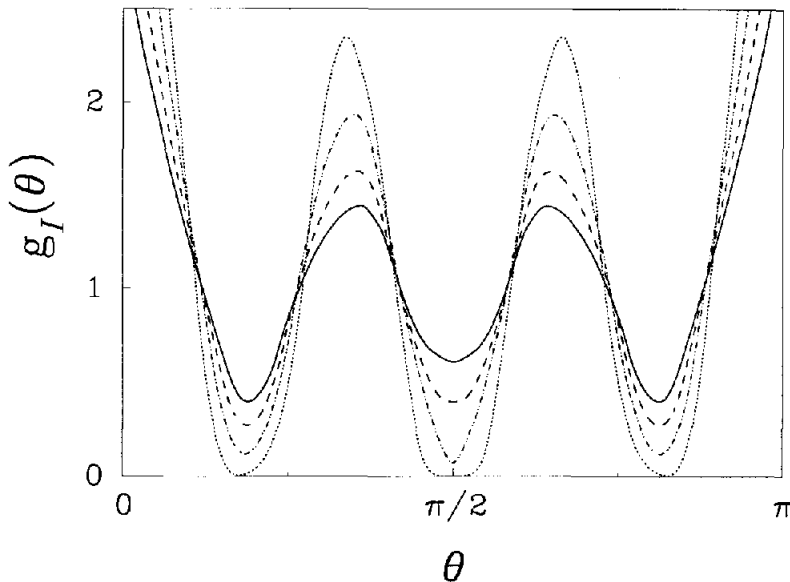


Fig. 9. Interstice radial distribution function $g_I(r)$ for matter distributed inside equal circular domains centred at the vertices of a dodecahedron inscribed within the sphere. The function is plotted as a function of $\theta = r/R$ for different values of the interstice fractional coverage η_I . Continuous line, $\eta_I = 0.342$ (i.e., domains tangent to each other); dashed line, $\eta_I = 0.300$; dash-dotted line, $\eta_I = 0.245$; dotted line, $\eta_I = 0.174$. In the last three cases circular domains do overlap.

their RDF reproduces (apart from a trivial rescaling) the complementary *interstice* RDF associated with the icosahedron as indeed follows from eq. (12). However, this situation is far from realistic since the fraction of defects at high density is very low. Therefore, we should consistently reduce the size of the domains. As a result, the profile of $g_D(r)$ promptly changes merging into that of defects confined in the *interstices* of a dodecahedron. In fact, a 20% contraction of the domain size is already sufficient to wash out the two specular maxima lying at $\pi/4$ and $3\pi/4$, respectively.

This last comparison, together with the invariance property exploited in fig. 9, shows that the icosahedral signature is largely independent on the fine geometrical details of the model called for to explain the long-wavelength modulation of the defect distribution function.

6. Concluding remarks

A Monte Carlo study of the statistical mechanics of a model system of hard particles under spherical boundary conditions [1] has been extended by carrying out a rather detailed analysis of defects. At high densities this system

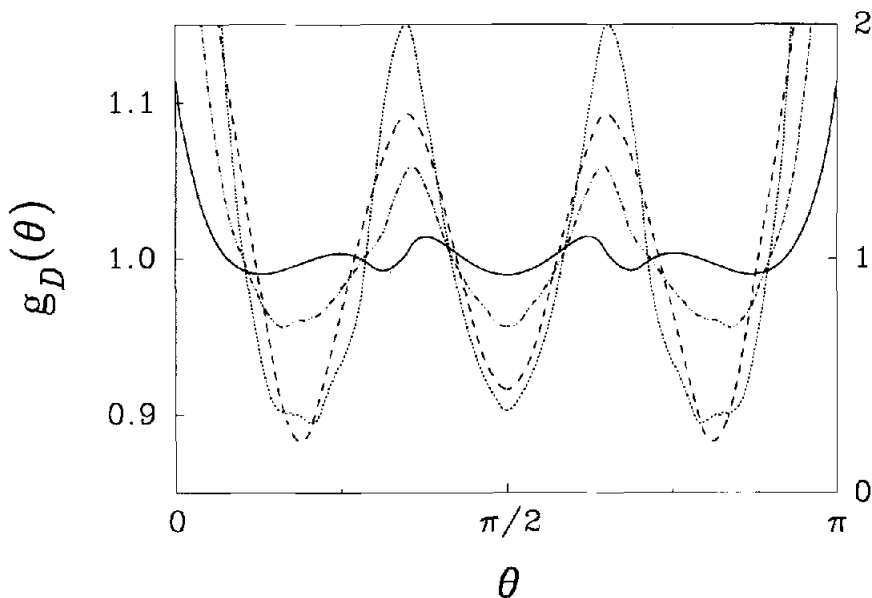


Fig. 10. Radial distribution function, plotted as a function of $\theta = r/R$, for a model distribution of defects uniformly dispersed inside equal circular domains centred at the vertices of an icosahedron inscribed within the sphere. The four curves refer to decreasing values of the domain fractional coverage η_D . Continuous line, $\eta_D = 0.896$ (i.e., domains tangent to each other); dash-dotted line, $\eta_D = 0.735$; dotted line, $\eta_D = 0.600$; dashed line, $\eta_D = 0.300$ (right axis).

undergoes a diffuse freezing transition in the range $0.83 \leq \rho\sigma^2 \leq 0.91$ which culminates with the formation of a large-scale superstructure. In fact, for densities larger than 0.91, most of the coordination defects appear to segregate into clusters which pin at the vertices of an icosahedron inscribed within the sphere.

As far as we know, it was Nelson who first suggested that at very low temperatures (or very high densities) excess disclinations on a surface with constant curvature would form a “crystalline superlattice” [4]^{#2}. This idea, which in the referred papers rested on plausibility arguments only, has been validated in this work through a numerical experiment. The crudeness of the hard-core model shows how the emergence of a rather complex pattern at high densities is the mere outcome of the principle of maximum entropy conjugated with the unusual topology of the sphere. In this case, such a principle is tantamount to a request of maximal efficiency in the way the free volume is distributed over the system.

^{#2} This idea is also shared by Straley [9]; a simplified geometrical argument leading to the same conclusion may be found in ref. [8].

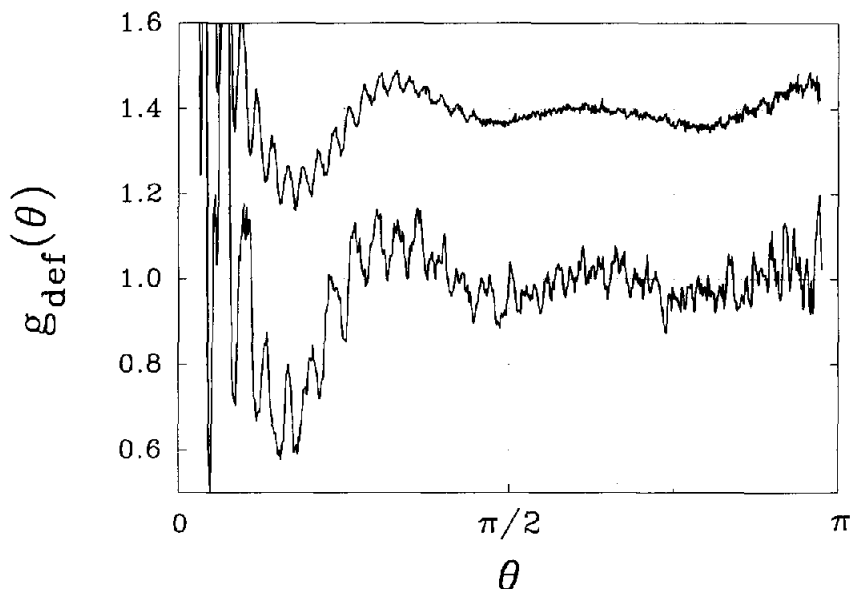


Fig. 11. Cumulative radial distribution function of defects plotted as a function of the angular distance $\theta = r/R$ for 1000 calottes at $\rho\sigma^2 = 0.95$ (lower curve) and for 2000 calottes at $\rho\sigma^2 = 0.925$ (upper curve). The second curve has been shifted upwards by 0.4 for clarity.

The solution exploited by the model for $N = 2000$ is the same observed in a system of 1000 calottes, as can be appreciated from fig. 11. However, one may actually wonder if this scenario changes on increasing the number of particles, i.e., on approaching the flat geometry limit. In fact, we recall that the size of the hexagonal domains enclosed within the icosahedral frame grows at the most as $N^{1/3}$, then much more slowly than the radius of the sphere [1]. Therefore, it is quite reasonable to expect the appearance of linear defects (dislocations or grain boundaries) inside each ordered domain whose role is that of soldering differently oriented patches. However, notwithstanding the internal “cracking” of the domains (which will reasonably lead to a finer modulation of the superstructure), we still believe that the icosahedral symmetry will persist in the large-scale aggregation of such composite domains. The icosahedral frame is somehow bound to bear the excess of 5 disclinations induced by the finite curvature of the surface (see section 3). In addition to this, one should expect a growth with N of dislocation pairs. In the long run, these defects, which have no disrupting effect on the ordered texture, will prevail over others, as also predicted by the KTHNY theory for the solid phase in Euclidean geometry.

In the light of the considerations developed above and in ref. [1], we surmise that the bounds of the “critical” density range identified in the system of 2000

calottes will eventually evolve into the two-phase boundary observed in a system of hard disks with periodic boundary conditions. At any rate, the discontinuous character credited by numerical simulation experiments to the freezing transition on a plane may be hardly harmonized with the present scheme. Indeed, a more conclusive statement on the nature of the transition undergone by the system in the thermodynamic limit cannot but come from a more extensive finite-size-scaling analysis of the model carried out for increasing values of the number of particles.

Acknowledgements

This work was supported by the Ministero dell'Università e della Ricerca Scientifica e Tecnologica, and by the Consorzio Interuniversitario Nazionale per la Fisica della Materia. The authors would also like to thank the Consiglio Nazionale delle Ricerche for the allocation of computer time via the Cray project on statistical mechanics.

References

- [1] S. Prestipino Giarritta, M. Ferrario and P.V. Giaquinta, *Physica A* 187 (1992) 456.
- [2] H.J.M. Hanley, T.R. Welberry, D.J. Evans and G.P. Morriss, *Phys. Rev. A* 38 (1988) 1628.
- [3] J.M. Kosterlitz and D.J. Thouless, *J. Phys. C* 6 (1973) 1181;
D.R. Nelson and B.I. Halperin, *Phys. Rev. B* 19 (1979) 2457;
A.P. Young, *Phys. Rev. B* 19 (1979) 1855.
- [4] D.R. Nelson, *Phys. Rev. B* 28 (1983) 5515.
- [5] C.A. Rogers, *Packing and Covering* (Cambridge Univ. Press, Cambridge, 1964).
- [6] H.S.M. Coxeter, *Regular Polytopes*, 2nd ed. (Macmillan, New York, 1963) p. 10.
- [7] C.A. Murray and D.H. Van Winkle, *Phys. Rev. Lett.* 58 (1987) 1200;
M.A. Glaser and N.A. Clark, *Phys. Rev. A* 41 (1990) 4585.
- [8] A.L. Mackay, J.L. Finney and K. Gotoh, *Acta Cryst. A* 33 (1977) 98.
- [9] J.P. Straley, *Phys. Rev. B* 30 (1984) 6592.